RSC Advances

PAPER

View Article Online
View Journal | View Issue

Cite this: *RSC Adv.*, 2016, **6**, 30176

Influence of the component interaction over Cu/ZrO_2 catalysts induced with fractionated precipitation method on the catalytic performance for methanol steam reforming

Jiajia Zhou,[a] Ye Zhang,[a] Guisheng Wu,*[a] Dongsen Mao*[a] and Guanzhong Lu[ab]

Received 25th November 2015
Accepted 3rd March 2016

DOI: 10.1039/c5ra24163d

www.rsc.org/advances

A series of binary Cu/ZrO_2 catalysts by choosing different composition ratios and different precipitation sequences have been prepared for the production of hydrogen by steam reforming of methanol (SRM). A variety of characterization techniques including N_2 adsorption, N_2O chemisorption, TEM, TPD and Raman are employed to characterize the physical and chemical properties of the catalysts. The results show that the preparation methods significantly affect the component dispersion, microstructure and adsorption properties. The Cu/ZrO_2 catalyst with 27.3% ZrO_2 loading prepared by fractionated precipitation method displays higher specific surface and interface between copper and zirconia, which not only accelerates decomposition of adsorbed methanol and water, but also promotes formation of Cu^+ and surface oxygen species, accordingly enhancing the catalytic activity and stability.

1. Introduction

The production of hydrogen by steam reforming of methanol (SRM) is of great importance for the development of fuel cell powered devices, especially for vehicles.[1] A large variety of catalytic materials containing the noble metals Pt, Pd, Rh[2–5] as well as transition metals Cu, Ni, Co[6–10] for the steam reforming of methanol have been reported in the literature. Among them, copper-based catalysts such as Cu/ZnO and Cu/ZnO/Al_2O_3 [11] have attracted the enormous interest for SRM reaction owing to their high activity and selectivity as well as their cheap price relative to noble-metal catalysts. Unfortunately, the shortcomings of poor catalytic stability and the by-product of a small amount of CO have limited their wide use in fuel cells. Therefore, promoting the catalytic stability and suppressing the production of CO are the crucial breakthroughs for the SRM over Cu-based catalysts.

During the last decades, copper supported on ZrO_2 has attracted considerable attention owing to its high activity, enhanced stability and lower CO production compared to conventional Cu supported on ZnO/ZnO–Al_2O_3 or SiO_2.[10,12–15] The promoted performance of zirconia-containing catalysts has been attributed to a higher Cu surface area, better Cu dispersion, and improved reducibility of Cu.[16,17] On the other hand, other factors apart from the essential nature of metallic copper should be taken into consideration for the catalytic production of hydrogen from methanol steam reforming. For example, Shimokawabe and co-workers[18,19] have demonstrated that although a high specific copper surface area is a prerequisite for catalytic activity, it does not account for the observed activity changes alone without taking the particular microstructure of the active Cu particles into account. Based on the corresponding relationship between catalyst activity and the surface oxygen content, Szizybalski *et al.*[20] and Oguchi *et al.*[21,22] believed that most Cu species were maintained in the transient valence state (Cu_2O) in the presence of a small amount of ZrO_2 and the oxygen species bonded with Cu^+ is the key factor affecting its activity for SRM. In addition, incorporation of Cu^+ cation into the ZrO_2 network compensates for the negative charge of vacancies and stabilizes the tetragonal ZrO_2 phase (t-ZrO_2),[23] which shows much higher catalytic activity for SRM than that with monoclinic zirconia (m-ZrO_2) as the support due to the high dispersed state of copper, and rich oxygen vacancies stabilized by Cu^+ ions in Cu/t-ZrO_2.[24] Therefore, the interface between copper and zirconia has been advanced to rationalize the high activity of Cu/ZrO_2 for methanol synthesis or methanol reforming because of the particular electronic interactions and synergistic effect of reaction species.[23,24] Although copper is regarded the active site and is supported over the surface of ZrO_2, accumulation of zirconia over Cu/ZrO_2 pretreated at high calcination or reduction temperature can promote the catalytic activity, in spite of the larger crystal size of copper or zirconia.[25] We have also reported that both model catalysts of ZnO/Cu and ZrO_2/Cu prepared by impregnated $Zn(NO_3)_2$ or $Zr(NO_3)_4$ over

[a]*Research Institute of Applied Catalysis, School of Chemical and Environmental Engineering, Shanghai Institute of Technology, Shanghai 201418, PR China. E-mail: gswu@sit.edu.cn; dsmao@sit.edu.cn*

[b]*Key Laboratory for Advanced Materials and Research Institute of Industrial Catalysis, East China University of Science and Technology, Shanghai 200237, PR China*

macro-size copper powder exhibited much higher catalytic activity and stability relative to pure Cu catalyst.[26]

In order to promote the performance of Cu/ZrO_2 catalysts for methanol synthesis or methanol reforming, various preparation methods, such as co-precipitation of metal salts,[27] impregnation of copper onto a zirconia support,[18,19] the formation of amorphous aerogels[28,29] and the polymer templating technique[30,31] have been proposed. A variety of different pretreatment processes including calcination or reduction at different temperatures,[25,32] or pretreatment with microwave irradiation[33] have also been put forward. Maintaining the high surface area by stabilizing the amorphous nature of zirconia or t-ZrO_2 phase under calcination and reaction conditions as well as maintaining a high copper/zirconia interfacial area has been found to be very important for the generation of highly active copper material with improved stability.[10] In view of active sites of Cu/ZrO_2 and preparation methods, efficient catalyst systems with cheap price and simple preparation process as well as high Cu–ZrO_2 interfacial area are highly desirable.

In the present work, in order to develop facile and efficient binary Cu/ZrO_2 catalysts with a high Cu/Zr interface and unique component interaction for methanol steam reforming, Cu/ZrO_2 catalysts prepared by fractionated precipitation method are chosen and compared with samples prepared by co-precipitation, and their performance in the SRM reaction is determined herein. Special attention is paid to the relationship between the catalytic performance and physicochemical properties such as the interaction between copper and zirconia species as well as the adsorption ability to methanol and water for the catalysts. In addition, the synergistic effects between Cu and ZrO_2 and the role of zirconia were discussed on the basis of TEM, TPD, Raman analyses and *in situ* diffuse reflectance infrared spectroscopy.

2. Experimental

2.1. Catalyst preparation

2.1.1 Co-precipitation method. Accurately measured stoichiometric aqueous mixtures of $Cu(NO_3)_2$ (A.R., Sinopharm Chemical Reagent Ltd.) and $ZrOCl_2$ (A.R., Sinopharm Chemical Reagent Ltd.) as well as of an aqueous solution of Na_2CO_3 (0.5 M, A.R., Sinopharm Chemical Reagent Ltd.) were added to the precipitating reactor under vigorous stirring at 60 °C, while the pH value of the reaction medium was kept at 9. Subsequently, these reaction media were aged under stirring for 1 h at 60 °C and cooled statically for 1 h. After filtration and washing with de-ionized water until the filtrate was neutral, the precursor was dried at 120 °C for 12 h, and calcined at 450 °C for 4 h.

2.1.2 Fractionated precipitation method. An aqueous solution of $Cu(NO_3)_2$ (0.5 M) and an aqueous solution of Na_2CO_3 (0.5 M) were added to the precipitating reactor under vigorous stirring at 60 °C and pH 7.5. Subsequently, a solution of $ZrOCl_2$ and a solution of Na_2CO_3 were added under the same precipitation conditions except that the pH was maintained at 9.0. The processing procedure of the suspension liquid was then the same as described above.

The prepared catalysts are labeled as CZ-*x*-*y*-c/f, in which $x : y$ represents the atomic ratio of copper and zirconium in Cu/ZrO_2 catalysts and c and f represent the coprecipitation and fractionated precipitation method, respectively. In addition, the pure copper catalyst prepared by precipitation is labeled as C-1-c.

2.2. Catalyst characterization

The metallic copper surface area (S_{Cu}) of the catalysts were determined using a nitrous oxide chemisorption method.[34] The catalyst samples (0.2 g) were reduced up to 280 °C in a 5% H_2/He stream (40 ml min^{-1}) for 1 h, and then were cooled to 60 °C in an He stream. Subsequently, a flow of 1% N_2O/He (1 ml min^{-1}) was passed through the sample with the temperature being maintained at 60 °C, while the signals of the thermal conductivity detector (TCD) signal were recorded. A surface copper atom density of 1.46×10^{19} m^{-2}, assuming $Cu : N_2O = 2 : 1$, was used for the calculation of the copper surface area.[35] The surface areas of the catalysts (S_{BET}) were measured by N_2 adsorption at −196 °C using a Micrometrics ASAP 2020 apparatus and calculated by the Brunauer–Emmett–Teller (BET) method.

Transmission electron microscopy (TEM) images were obtained using a FEIG2F30 microscope operated at 100 kV. The samples were suspended in ethanol and supported onto a holey carbon film on a Cu grid.

Temperature programmed desorption (TPD) of methanol and water was performed in a quartz tube reactor system equipped with a quadrupole mass spectrometer (QMS200, Balzers OmniStar) under atmospheric pressure. A 100 mg sample in 40–60 mesh was reduced in a 5% H_2/He flow (40 ml min^{-1}) at 280 °C for 1 h and then cooled to room temperature in 40 ml min^{-1} He flow. Subsequently, a flow of a mixture (40 ml min^{-1}) of methanol vapour and He was passed through the sample for 60 min, ensuring saturated adsorption of methanol over the catalysts. After that, the sample was swept with a 40 ml min^{-1} He stream, until no signals of methanol was determined. Finally, the sample was heated in 40 ml min^{-1} He flow from ambient temperature to 700 °C at a ramping rate of 15 °C min^{-1}. The *m*/*z* signals of 2, 28, 28, 30, 32 and 44 corresponding to H_2, CO, CH_2O, CH_3OH and CO_2 were monitored by an on-line quadrupole mass spectrometer. With regards to TPD of water, adsorption of steam and purging with He flow were carried out at 230 °C and the *m*/*z* signal of 18 corresponding to H_2O was monitored in order to follow the adsorption and activation of water at the reaction temperature of SRM.

In situ diffuse reflectance infrared spectroscopy was performed using a Nicolet 6700 FTIR spectrometer. The powdered samples were held in a Harrick Scientific (HS) high-temperature reaction chamber, the temperature of which was controlled by a HSI temperature controller. The samples was reduced at 300 °C in 5% H_2/N_2 flowing at 50 ml min^{-1} for 30 min. After cooling to room temperature in an N_2 purge at 50 ml min^{-1}, the samples were pumped to 1×10^{-2} Pa, and then the spectra of the background was collected. Subsequently, about 20 ml CO (0.1 MPa) was introduced by one pulse injection and then the

adsorption timer started. *In situ* absorbance spectra were referenced to a spectrum of the background described earlier by collecting 64 scans at 4 cm^{-1} resolution.

Raman spectra were recorded using a DXR Raman spectrometer equipped with a ~100 mW, 785 nm diode laser. The powdered samples were held in a Harrick Scientific (HS) high-temperature reaction chamber, the temperature of which was controlled by a HSI temperature controller. The surface species over the samples reduced at different times at 300 °C, as well as exposed to steam for 30 h at 230 °C, were monitored online using Raman spectroscopy.

2.3. Catalytic activity testing

The catalytic activities were tested in a fixed-bed reactor under atmospheric pressure. 0.5 g sample of the catalyst was reduced in a 5% H_2/N_2 flow (50 ml min^{-1}) at 280 °C for 1 h and then cooled to 230 °C in N_2 flow. After that, a mixture of water and methanol with a volume ratio of 1.2 fed into by an injection pump was preheated to about 200 °C to ensure full vaporization before being introduced in the reactor. The tail gas from the reactor was passed through a cold trap cooling with an ice-water bath, and then was analyzed on-line by a gas chromatograph (GC 2060) equipped with thermal conductivity detectors and TDX-01 column; the liquid products such as water, methanol were detected by the same gas chromatograph equipped with thermal conductivity detectors and a Porapak-Q column.

3. Results

In order to illustrate the effect of ZrO_2 on the catalytic activity over Cu/ZrO_2, Fig. 1 shows the variation trends of catalytic activity and CO selectivity with different ZrO_2 loadings as well as different preparation methods. It is clear that the ZrO_2 loading has a significant influence on the performance of Cu/ZrO_2 for hydrogen production from steam reforming of methanol. At first, the catalytic activity and selectivity of Cu/ZrO_2 prepared by fractionated precipitation are compared. C-1-c reveals low catalytic activity with 32.4% of methanol conversion and 0.046 mol $gcat^{-1}$ h^{-1} of hydrogen production rate. With increase of ZrO_2 loading, the methanol conversion and hydrogen production rate increase remarkably and achieve the highest values over CZ-8-3-f which contains 27.3% of ZrO_2.

With a further increase of ZrO_2 content, the catalytic activity drops significantly and CZ-8-8-f shows 30% methanol conversion and 0.041 $gcat^{-1}$ h^{-1} of hydrogen production rate. As a comparison, the activity results of catalysts prepared by co-precipitation methods are also shown in Fig. 1. When ZrO_2 loading is low, Cu/ZrO_2 prepared by fractionated precipitation shows higher activity, while samples prepared by co-precipitation show higher performance with higher ZrO_2 content. For example, comparing methanol conversion, it is found that CZ-8-3-f presents 92% and CZ-8-3-c 67%, whereas CZ-8-8-f displays 30% but CZ-8-8-c 80%.

For all catalysts, the selectivity of CO_2 first increased and then decreased with the content of ZrO_2, moreover, CO selectivity over all catalysts is maintained below 1.5%.

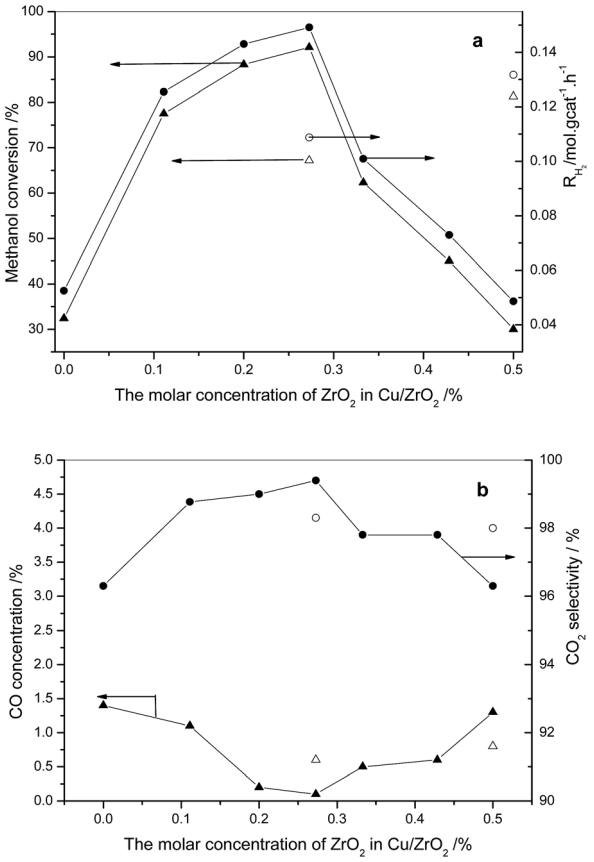

Fig. 1 Effects of ZrO_2 loadings on catalytic activity over CZ catalysts prepared by different methods. Circles in (a) and (b) represent the production rate of H_2 and CO_2 selectivity, respectively, while the triangles in (a) and (b) represent the methanol conversion and the volumetric CO content in the outlet, respectively. Solid and hollow symbols represent the data over CZ catalysts prepared by fractionated precipitation and co-precipitation, respectively (reaction conditions: $T = 230$ °C, $p = 0.1$ MPa, $H_2O/CH_3OH = 1.2$ molar ratio, WHSV = 4.8 ml $gcat^{-1}$ h^{-1}).

It is well known that the main shortcoming of Cu based catalysts in SRM is the fast deactivation with time-on-stream. The catalytic stabilities of the SRM reaction over C-1-c as well as CZ-8-3-c and CZ-8-3-f were investigated for 24 h at 230 °C (Fig. 2). The activity of C-1-c lasts for about 2.5 h and then steadily drops to zero after 10 h. The methanol conversion of CZ-8-3-c is maintained at about 71% for the first 5 h, and then begins to slightly decline continuously, finally reaching 65% at the end of 24 h of time-on-stream. For the catalyst CZ-8-3-f, no appreciable decrease in the activity is observed after 24 h of time-on-stream, suggesting excellent catalytic stability of Cu/ZrO_2 is obtained from fractionated precipitation. Yao *et al.*[36] also obtained Cu/ZrO_2 catalysts for MSR through oxalate gel-co-precipitation with highly dispersed catalytic components of copper and zirconia, which could maintain high activity at 300 °C for 48 h. Purnama *et al.*[37] have investigated the deactivation behavior of a template-derived Cu/ZrO_2, and found that a much smaller extent of deactivation was identified for Cu/ZrO_2 relative to commercial CuZnAl catalysts, and attributed the high

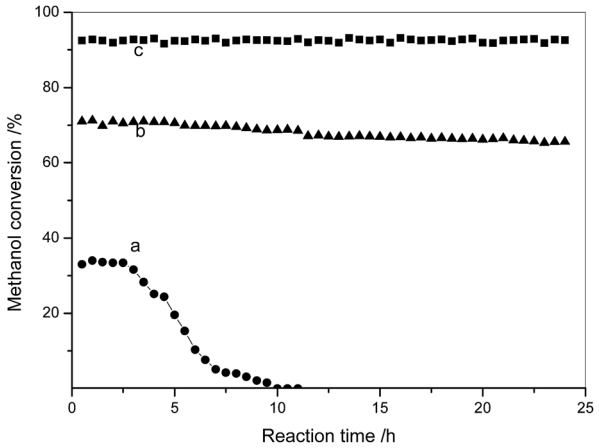

Fig. 2 Methanol conversions over C-1-c (a), CZ-8-3-c (b) and CZ-8-3-f as a function of time-on-stream (reaction conditions: $T = 230$ °C, $p = 0.1$ MPa, $H_2O/CH_3OH = 1.2$ molar ratio, WHSV = 4.8 ml gcat^{-1} h^{-1}).

stability to the fact that the copper particles in the zirconia catalyst were well dispersed and stabilized. Table 1 summarizes the specific surface areas and Cu metal surface areas measured by nitrous oxide titration of the Cu/ZrO_2 catalysts with different ZrO_2 loadings as well as different preparation methods. It is clear that C-1-c shows 8.1 m^2 g^{-1} BET specific surface and 1.0 m^2 g^{-1} Cu metal surface area. The specific surface area of Cu/ZrO_2 increased significantly to 41.0 m^2 g^{-1} with introduction of 11.1% ZrO_2, and further continuously increased with an increase of ZrO_2 loading. On the other hand, the copper surface area increased with addition of ZrO_2 from 11.1 to 27.3% and then decreased with further increase of ZrO_2. Considering the fact that CZ-8-3-f with 27.3% ZrO_2 shows the highest activity for MSR, one can conclude that both the copper surface area and the specific surface area should be taken into account for the catalytic activity.

The digital micrographs of two Cu/ZrO_2 samples prepared by different methods are shown in Fig. 3. It is clear that the precipitation methods have a great influence on the particle size and the distribution of catalysts. Among the two samples, CZ-8-3-c exhibits uniform size distribution with some compact structures. However, larger particles with loose structure are observed in CZ-8-3-f. Hence Cu/ZrO_2 catalyst prepared by

Table 1 Textural properties of Cu/ZrO_2 prepared by different methods

Sample	Molar content of zirconia (%)	S_{BET}/m^2 g^{-1}	S_{Cu}/m^2 g^{-1}
C-1-c	0.0	8.1	1.0
CZ-8-1-f	11.1	41.0	2.71
CZ-8-2-f	20.0	70.0	5.49
CZ-8-3-c	27.3	65.9	4.62
CZ-8-3-f	27.3	75.5	7.97
CZ-8-4-f	33.3	73.7	7.03
CZ-8-6-f	42.9	83.5	5.93
CZ-8-8-f	50.0	85.2	4.51

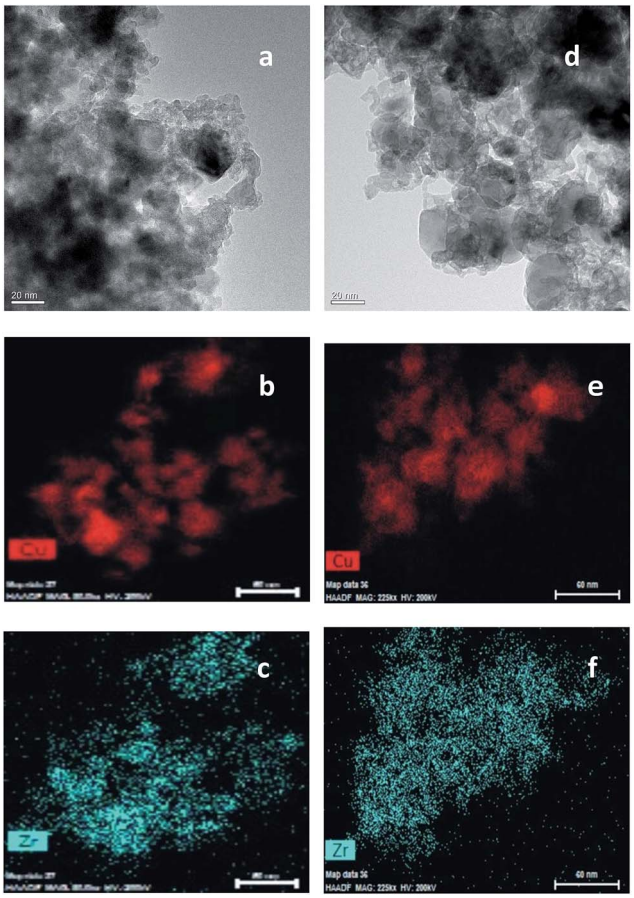

Fig. 3 TEM images of CZ-3-8-c (a) and CZ-3-8-f (d). Based on energy spectrum analysis, the copper distribution maps in CZ-3-8-c (b) and CZ-3-8-f (e) as well as the zirconium distribution maps in CZ-3-8-c (c) and CZ-3-8-f (f) are also shown.

fractionated precipitation method shows looser structure which can increase the specific surface significantly and matches with the results of BET surface area. Furthermore, the component distribution maps reveal that Cu and Zr are well dispersed in CZ-8-3-f.

In spite of the importance of specific area and copper area to the catalytic activity, they alone cannot fully explain the performance. In order to illustrate the effect of interface between copper and zirconia, the adsorption performance of methanol and water over Cu and Cu/ZrO_2 are further compared.

The TPD profiles of methanol over C-1-c, ZrO_2 and CZ-8-3-f are shown in Fig. 4, which reveals the different desorption behavior of methanol over the different catalysts. C-1-c shows weak adsorption ability, illustrated by the fact that a small amount of methanol and CO_2 is desorbed below 200 °C, and the weak and broad desorption peaks of H_2 and formaldehyde simultaneously appear in the range of 200–400 °C. With regard to pure ZrO_2, apart from the desorption of methanol from ambient temperature to 500 °C, strong desorption peaks ascribed to CO and H_2 were observed centered at 500 °C. Over CZ-8-3-f, however, the desorption temperature of CO and H_2 decreased to 370 °C, and furthermore, the desorption peak of

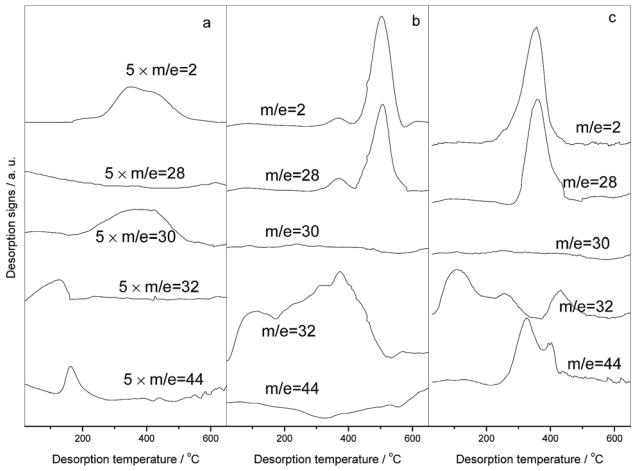

Fig. 4 TPD patterns of methanol on C-1-c (a), ZrO_2 (b) and CZ-8-3-f (c); peaks at m/z = 2, 28, 30, 32, 44, correspond to the desorbed species H_2, CO, CH_2O, CH_3OH, CO_2, respectively. Due to the weak desorption over C-1-c, all desorption signs over C-*a*-c are magnified by 5 times.

CO_2 was also observed in this temperature range. These results illustrate that the combination of copper and zirconia can accelerate the decomposition of methanol to produce CO and H_2, and promote the formation of CO_2.

Besides the adsorption of methanol, the adsorption and activation of the water are of importance to the MSR, hence TPD profiles of water over C-1-c and CZ-8-3-f are shown in Fig. 5. It is clear that C-1-c displayed poor adsorption capacity and no perceptible water desorption peaks are observed. In contrast, a strong desorption signal of water is observed in the temperature range of 350–600 °C over CZ-8-3-f. It is surprising that the desorption of water occurs around 400–600 °C, which might be due to dehydration of adjacent hydroxyl produced by the dissociative adsorption of water over Cu/ZrO_2. These results illustrate that Cu/ZrO_2 shows much stronger adsorption towards water than Cu at the reaction temperature, which might account for the high activity of Cu/ZrO_2 for MSR.

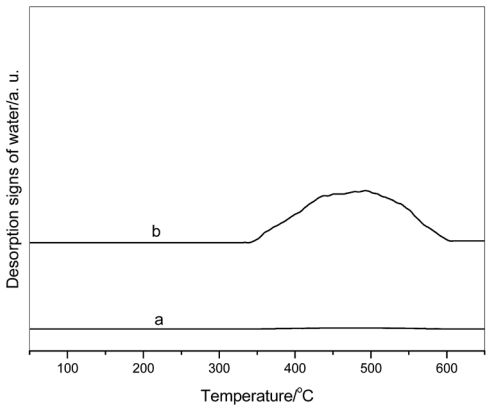

Fig. 5 TPD profiles of water over C-1-c (a) and CZ-8-3-f (b).

In order to further investigate the Cu species over the catalysts, CO adsorption is measured with an *in situ* diffuse reflectance infrared spectroscopy, as shown in Fig. 6. When CO was adsorbed over C-1-c, only a weak band centered about 2146 cm^{-1} ascribed to the C–O stretching vibration of gaseous CO was observed, and its intensity did not show any change with the adsorption time, illustrating the low adsorption ability of CO over unsupported Cu catalysts. With regards to CZ-8-3-c, the bands at 2098 and 2133 cm^{-1}, ascribed to CO adsorbed linearly on high-index planes of metallic Cu and Cu^+,[38] respectively, appeared at the same time, which increased initially and then remained unchanged in intensity with adsorption time. When CO was adsorbed over CZ-8-3-f, much stronger bands at 2105 and 2131 cm^{-1} were displayed relative to CZ-8-3-c, furthermore, the intensity of the former deceased while that of the latter increased with the adsorption time. Those findings indicate that CZ-8-3-f not only shows the strong adsorption ability to CO at the active sites of Cu^0 and Cu^+, but also exhibits the CO spillover from Cu^0 to Cu^+.

The surface species of C-1-c and CZ-8-3-f in the process of reduction as well as the adsorption of water are also characterized by Raman spectroscopy, and are shown in Fig. 7. C-1-c displayed three peaks at 291, 335 and 626 cm^{-1}, which is ascribed to A_g, B_g^1 and B_g^2 of the Raman-active phonon modes in the C_{2h}^6 point group of monoclinic bulk CuO.[39,40] After reduction in hydrogen at 300 °C for 30 min, no evident change is observable with regard to Raman spectra, illustrating that the main surface species over copper is still CuO. When the reduction time reached 60 min, the characteristic bands of CuO

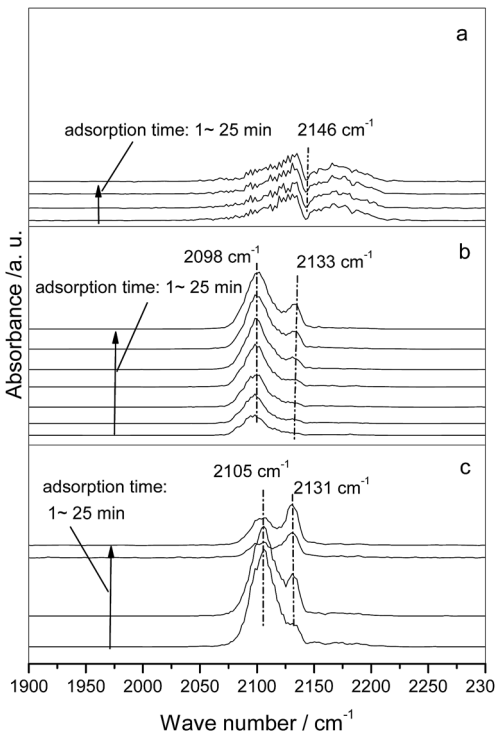

Fig. 6 Infrared spectra of CO adsorption over C-1-c (a), CZ-8-3-c (b) and CZ-8-3-f (c).

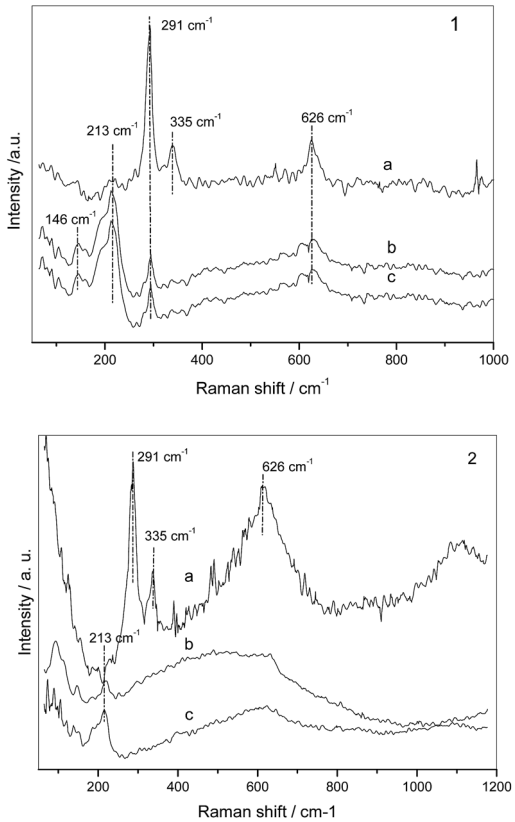

Fig. 7 Raman spectra of C-1-c (1) and CZ-8-3-f (2) recorded at different conditions. Both samples are shown as prepared (a) and reduced at 300 °C for 0.5 h (CZ-8-3-f, (b)) or 1 h (C-1-c, (b)), and then exposed in steam at 230 °C for 30 min (c).

decreased significantly and two bands at 146 and 213 cm^{-1}, which are attributed to the Raman-active phonon modes of Γ_{15}^{-} and $2\Gamma_{12}^{-}$ in crystalline Cu_2O,[41,42] emerge. Upon exposure to steam for 30 min, the surface species over C-1-c remain unchanged. Concerning CZ-8-3-f, only broad bands ascribed to CuO are observed in Fig. 7, but bands attributed to crystalline ZrO_2 are not found, indicating that the crystal size of CuO became small with introduction of ZrO_2 and that ZrO_2 species is highly dispersed or is in the form of an amorphous state. After reduction in hydrogen at 300 °C for 30 min, the bands of CuO disappeared completely and only a weak band at 213 cm^{-1} ascribed to Cu_2O appeared. After introducing steam, however, the band ascribed to Cu_2O increased. These results illustrate that CuO species in pure CuO particles is difficult to reduce and then dominant species are Cu_2O as well as CuO. By contrast, Cu/ZrO_2 is much more easily reduced to Cu^0, hence only a small amount of Cu_2O remained after reduction at 300 °C for 30 min. The fact that ZrO_2 can promote the reduction of CuO can also be evidenced by TPR results.[12,36] IR results of CO adsorption shows that Cu^+ is stabilized on the interface between copper and zirconia, as also is evidenced by Auger and XPS[23] spectroscopic studies and X-ray absorption fine structure analysis.[24] Furthermore, ZrO_2 in Cu/ZrO_2 can also promote the adsorption and activation of water and formation of Cu^+, by a mechanism as proposed as shown in Scheme 1:

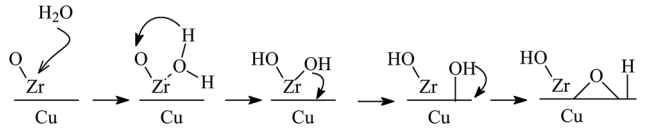

Scheme 1

The water is adsorbed on the oxygen vacancy sites of zirconia and further dissociated and bonded with adjacent oxygen atom to form two hydroxyls. The formed hydroxyl over ZrO_2 can spillover to the surface of copper and subsequently is dehydrogenated to form surface oxygen species and Cu species.

4. Discussion

It is well known that a variety of factors affect the catalytic activity of Cu/ZrO_2, including physical properties, such as the specific area of catalyst, copper surface area, the crystal size distribution and the morphology of Cu/ZrO_2, as well as the chemical interaction between copper and zirconia.[10–19,36] Despite the various preparation methods of Cu/ZrO_2, a clear aim of almost all preparation methods is to increase the specific area of Cu/ZrO_2 as well as the surface area of Cu,[28] and to promote the interaction between copper and zirconia[23,24] by improving copper dispersion in ZrO_2 and maintaining the amorphous nature. In our study, the fractionated precipitation method enhances the specific surface area as well as copper surface area of Cu/ZrO_2 effectively. Comparing the preparation conditions, Cu^{2+} precipitates at pH of 7.5[43] while the sol–gel containing Zr^{4+} is formed at pH about 9–10.[44] In the process of co-precipitation of Cu^{2+} and Zr^{4+}, Cu^{2+} is rapidly precipitated to form crystal nuclei at pH 9, which can accelerate precipitation of Zr^{4+} and hinder the formation of sol–gel containing Zr^{4+}, therefore the particle size shown in TEM is small but compact. In the process of fractionated precipitation, however, Cu^{2+} is precipitated at low pH (7.5) to form a superfine copper precipitate, subsequently, Zr^{4+} precipitated at higher pH (9) to form a sol–gel, which can effectively adsorb and envelope the precipitate containing copper. After drying and calcination, large particles with loose structure are formed, which can be beneficial to increase the specific area as well as the copper surface area of Cu/ZrO_2. At the same time, owing to the highly dispersed state of copper and zirconia, a large amount of Cu^+ is formed on the interface of CZ-8-3-f between copper and zirconia, which not only hinders aggregation of copper and crystallization of zirconia,[28] but also maintains the catalytic stability and suppresses production of CO.[12,28] Therefore, CZ-8-3-f shows much higher activity and stability than copper or CZ-8-3-c. When ZrO_2 loading reaches 50%, in spite of the much larger surface area of CZ-8-8-f, its activity is lower than that of C-1-c, but CZ-8-8-c showed much higher activity. We can envisage that a high content of ZrO_2 leads to accumulation on the surface of Cu/ZrO_2, and then copper species is blocked from contacting with reactants; illustrating that copper is also crucial to catalytic activity.

On the other hand, it is also believed that the interaction between copper and zirconia rather than the specific surface area should explain the high activity of Cu/ZrO_2 because of the unique role of ZrO_2 such as acidity and basicity as well as strong adsorption properties. Therefore, the copper and ZrO_2 species over the catalysts are proposed to behave in a bifunctional manner, with copper and ZrO_2 playing synergetic roles in methanol synthesis reaction or methanol decomposition.[36,45] Among them, methanol interacts with the OH groups over ZrO_2 to form methoxide, which can decompose to CO and H_2 *via* formaldehyde from methoxide dehydrogenation, while copper is proposed to accept the hydrogen spilled from the surface species located on ZrO_2 to form molecular hydrogen.[36] In addition, the spillover between copper and zirconia is also of importance to the catalytic activity.[46] The results of TEM and Raman in the present work show that, for Cu/ZrO_2 prepared by fractionated precipitation, the copper and zirconia components are well dispersed with each other and loose microstructure and morphography are formed, which not only increase the specific area of the catalysts, but also strengthen the interaction between copper and zirconia. IR adsorption of CO adsorption over Cu/ZrO_2 furthermore illustrates that CZ-8-3-f shows facile CO spillover from Cu^0 to Cu^+ due to a much higher interfacial contact between copper and zirconia and more stabilized Cu^+ species. The methanol-TPD results reveal that, moreover, Cu/ZrO_2 shows desorption peaks of CO and H_2 at much lower temperature than pure ZrO_2, aside from exhibiting the desorption peaks of CO_2, but C-1-c only shows weak desorption of formaldehyde, hydrogen, CO_2 and methanol. These results provide further evidence for the synergistic effect between copper and zirconia, indicating that zirconia not only serves as a support for copper, but also plays the role to activate sites towards decomposition of adsorbed methanol and water.

The fact the Cu/ZrO_2 catalyst reduced in hydrogen showed initially low activity for MSR and promoted activity with exposure to oxygen[20] indicates that oxygen is also a key factor to promote the catalytic activity for MSR. Oguchi *et al.*[21,22] further confirmed this view through the evidence of the approximate linear relation between the H_2 production rate and surface oxygen content over Cu/ZrO_2. Raman results herein reveal that the surface of Cu contains rich Cu^+ species even when reduced at 300 °C for 60 min, hence it displayed certain initial activity. The transient stability of copper catalyst for MSR seems to be ascribed to the depletion of oxygen species over copper with reaction time because of its low adsorption ability towards water. Despite the majority of Cu species over Cu/ZrO_2 being reduced to Cu^0 after reduction for 30 min, surface Cu^+ species is enhanced after adsorption of water indicating that the interface between copper and zirconia can promote surface hydroxyl groups over ZrO_2 obtained from dissociative adsorption of water to spillover to the surface of copper, subsequently the hydroxyl over copper is further dehydrogenated to form the surface oxygen species, and accordingly CZ-8-3-f shows the optimum catalytic activity and stability. When water is introduced over $Cu/CeO_2/Al_2O_3$[47] or Co/ZrO_2, it is also found that Cu^0 is oxidized to Cu^+ or the content of Co^0 is reduced.[48]

In addition, surface science experiments[49] also revealed that methanol on clean single-crystal Cu surfaces tends to show little or no reactivity and surface oxygen must exist on the surface of Cu crystal surface in order to facilitate the adsorption of methanol. Based on the physical properties of Cu, it is clear that a low specific area and nonpolar surface of clean copper metal results in low adsorption activation towards methanol or water. Furthermore, the electron in the 5s orbital of Cu^0 presents a repulsive interaction to the lone electron pair of oxygen in methanol or water, which further hinders dissociative adsorption of them on the surface of Cu. However, Cu^+ species with a vacant 5s orbital not only interacts with the lone electron pair of oxygen in methanol, but also provides an occupied symmetry-adapted d orbital which can be activated towards methanol by feedback of d electrons to the antibonding orbital of methanol to form methoxide intermediate as well as formaldehyde. In Cu/ZrO_2, bonded with oxygen ions over ZrO_2, copper atoms are highly dispersed in ZrO_2 and tend to be oxidized to higher valence, and then show higher activity to methanol.

5. Conclusion

A series of binary Cu/ZrO_2 catalysts by choosing different composition ratios and different precipitation sequences have been prepared for the steam reforming of methanol (SRM), and it is shown that the Cu/ZrO_2 catalyst with 27.3% ZrO_2 introduced by fractionated precipitation method shows the best activity and stability. The characterization results including N_2 adsorption, N_2O chemisorption and TEM, illustrate that CZ-8-3-f has a large metallic copper surface area as well as a high component dispersion. The results of TPD and Raman reveal a synergic effect between copper and zirconia illustrated by the fact that methanol adsorption and decomposition were accelerated and Cu^+ was formed by adsorption of water over ZrO_2, which further illustrates the high activity and stability of CZ-8-3-f for the steam reforming of methanol.

Acknowledgements

Financial support from the National Science Foundation of China (Grant No. 20503005), Shanghai Leading Academic Discipline Project (P1501) and the program of Shanghai municipal Education commission, China are gratefully acknowledged.

Notes and references

1 J. Agrell, M. Boutonnet and J. L. G. Fierro, *Appl. Catal., A*, 2003, **253**, 213.
2 N. Iwasa and N. Takezawa, *Appl. Catal., A*, 1995, **125**, 145.
3 M. L. Cubeiro and J. L. G. Fierro, *J. Catal.*, 1998, **179**, 150.
4 N. Iwasa and N. Takezawa, *Catal. Lett.*, 1998, **54**, 119.
5 N. Takezawa and N. Iwasa, *Catal. Today*, 1997, **36**, 45.
6 Y. Matsumura, *Int. J. Hydrogen Energy*, 2013, **38**, 13950.
7 T. L. Reitz, S. Ahmed and M. Krumpelt, *J. Mol. Catal. A: Chem.*, 2000, **162**, 275.

8 N. Takezawa, H. Kobayashi, A. Hirose and M. Shimokawabe, *Appl. Catal.*, 1982, **4**, 127.
9 A. A. G. Lima, M. Nele, E. L. Moreno and H. M. C. Andrade, *Appl. Catal., A*, 1998, **171**, 31.
10 J. P. Breen and J. R. Ross, *Catal. Today*, 1999, **51**, 521.
11 S. T. Yong, C. W. Ooi, S. P. Chai and X. S. Wu, *Int. J. Hydrogen Energy*, 2013, **38**, 9541.
12 G. Huang, B. Liaw, C. Jhang and Y. Chen, *Appl. Catal., A*, 2009, **358**, 7.
13 Y. Matsumura and H. Ishibe, *J. Mol. Catal. A: Chem.*, 2011, **345**, 44.
14 S. D. Jones and H. E. Hagelin-Weaver, *Appl. Catal., B*, 2009, **90**, 195.
15 S. G. Sanches, J. Huertas Flores, R. R. de Avillez and M. I. Pais da Silva, *Int. J. Hydrogen Energy*, 2012, **37**, 6572.
16 P. H. Matter, D. J. Braden and U. S. Ozkan, *J. Catal.*, 2004, **223**, 340.
17 V. Ramaswamy, M. Bhagwat, D. Srinivas and A. V. Ramaswamy, *Catal. Today*, 2004, **97**, 63.
18 M. Shimokawabe, H. Asakawa and N. Takezawa, *Appl. Catal.*, 1990, **59**, 45.
19 N. Takezawa, N. Shimokawabe, H. Hiramatsu, H. Sugiura, T. Asakawa and H. Kobayashi, *React. Kinet. Catal. Lett.*, 1987, **33**, 191.
20 A. Szizybalski, F. Girgsdies, A. Rabis, Y. Wang, M. Niederberger and T. Ressler, *J. Catal.*, 2005, **233**, 297.
21 H. Oguchi, H. Kanai, K. Utani, Y. Matsumura and S. Imamura, *Appl. Catal., A*, 2005, **293**, 64.
22 H. Oguchi, T. Nishiguchi, T. Matsumoto, H. Kanaia, K. Utani, Y. Matsumura and S. Imamura, *Appl. Catal., A*, 2005, **281**, 69.
23 K. Samson, M. Śliwa, R. P. Socha, K. Góra-Marek, D. Mucha, D. Rutkowska-Zbik, J.-F. Paul, M. Ruggiero Mikołajczyk, R. Grabowski and J. Słoczyński, *ACS Catal.*, 2014, **4**, 3730.
24 V. P. Pakharukova, E. M. Moroz, V. V. Kriventsov, T. V. Larina, A. I. Boronin, L. Y. Dolgikh and P. E. Strizhak, *J. Phys. Chem. C*, 2009, **113**, 21368.
25 G. Wu, Y. Sun, Y. Li, H. Jiao, H. Xiang and Y. Xu, *THEOCHEM*, 2003, **626**, 287.
26 G. Wu, D. Mao, G. Lu, Y. Cao and K. Fan, *Catal. Lett.*, 2009, **130**, 177.
27 R. A. Koeppel, A. Baiker and A. Wokaun, *Appl. Catal., A*, 1992, **84**, 77.
28 S. Esposito, M. Turco, G. Bagnasco, C. Cammarano, P. Pernice and A. Aronne, *Appl. Catal., A*, 2010, **372**, 48.
29 S. Velu, K. Suzuki, M. Okazaki, M. P. Kapoor, T. Osaki and F. Ohashi, *J. Catal.*, 2000, **194**, 373.
30 P. Rouhani, E. Salahinejad, R. Kaul, D. Vashaee and L. Tayebi, *J. Alloys Compd.*, 2013, **568**, 102.
31 D. Dipak, L. Jordi, M. Dominguez, C. Sara, T. Alessandro and G. Arup, *Int. J. Hydrogen Energy*, 2015, **40**, 10463.
32 Y. Choi, K. Futagami, T. Fujitani and J. Nakamura, *Appl. Catal., A*, 2001, **208**, 163.
33 X. Zhang, L. Wang, Y. Cao, W. Dai, H. He and K. Fan, *Chem. Commun.*, 2005, 4104.
34 R. T. Figueiredo, H. M. C. Andrade and J. L. Fierro, *J. Mol. Catal. A: Chem.*, 2010, **318**, 15.
35 G. C. Chinchen, C. M. Hay, H. D. Vandervell and K. C. Waugh, *J. Catal.*, 1987, **103**, 79.
36 C. Yao, L. Wang, Y. Liu, G. Wu, W. Dai, H. He and K. Fan, *Appl. Catal., A*, 2006, **297**, 151.
37 H. Purnama, F. Girgsdies, T. Ressler, J. H. Schattka, R. A. Caruso, R. Schomacker and R. Schlogl, *Catal. Lett.*, 2004, **94**, 61.
38 I. A. Fisher and A. T. Bell, *J. Catal.*, 1998, **178**, 153.
39 J. Chrzanowski and J. C. Irwin, *Solid State Commun.*, 1989, **70**, 11.
40 T. Yu, X. Zhao, Z. X. Shen, Y. H. Wu and W. H. Su, *J. Cryst. Growth*, 2004, **268**, 590.
41 G. Niaura, *Electrochim. Acta*, 2000, **45**, 3507.
42 C. A. Melendres, S. Xu and B. Tani, *J. Electroanal. Chem.*, 1984, **162**, 343.
43 Z. Shi, X. Xiao, D. Mao and G. Lu, *Catal. Sci. Technol.*, 2014, **4**, 1132.
44 B. Tyagi, K. Sidhpuria, B. Shaik and R. V. Jasra, *Ind. Eng. Chem. Res.*, 2006, **45**, 8643.
45 Y. Sun and P. A. Sermon, *J. Chem. Soc., Chem. Commun.*, 1993, 1242.
46 K. Jung and A. T. Bell, *J. Catal.*, 2000, **193**, 207.
47 M. Turco, G. Bagnascoa, C. Cammaranoa, L. Micoli, M. Lenardab, E. Moretti, L. Storaro and A. Talon, *Appl. Catal., B*, 2011, **102**, 387.
48 J. Sun, A. M. Karim, D. Mei, M. Engelhard, X. Bao and Y. Wang, *Appl. Catal., B*, 2015, **162**, 141.
49 C. Ammon, A. Bayer, G. Held, B. Richter, T. Schmidt and H.-P. Steinruck, *Surf. Sci.*, 2002, **507–510**, 845.